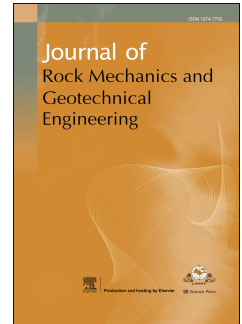# Journal Pre-proof

A method to experimentally investigate injection-induced activation of fractures

Changdong Ding, Yang Zhang, Qi Teng, Dawei Hu, Hui Zhou, Jianfu Shao, Chuanqing Zhang

Please cite this article as: Ding C, Zhang Y, Teng Q, Hu D, Zhou H, Shao J, Zhang C, A method to experimentally investigate injection-induced activation of fractures, *Journal of Rock Mechanics and Geotechnical Engineering*, https://doi.org/10.1016/j.jrmge.2020.04.002.

Journal of Rock Mechanics and Geotechnical Engineering

Journal online: www.rockgeotech.org

A method to experimentally investigate injection-induced activation of fractures

Changdong Ding[a,b], Yang Zhang[c], Qi Teng[d], Dawei Hu[a,b,*], Hui Zhou[a,b], Jianfu Shao[e], Chuanqing Zhang[a,b]

[a] *State Key Laboratory of Geomechanics and Geotechnical Engineering, Institute of Rock and Soil Mechanics, Chinese Academy of Sciences, Wuhan, 430071, China*

[b] *University of Chinese Academy of Sciences, Beijing, 100049, China*

[c] *CNPC Engineering Technology R&D Company Limited, Beijing, 102206, China*

[d] *PetroChina Tarim Oilfield Company, Korla, 841000, China*

[e] *University of Lille, LaMcube, CNRS FRE2016, 59000 Lille, France*

Abstract: Natural fractures are generally well developed in most hydrocarbon and geothermal reservoirs, which can produce complex fracture networks due to the activation of fractures during hydraulic stimulation. The present paper is devoted to developing a method to investigate the activation characteristics of fracture under injection-shearing coupled condition at laboratory scale. The fluid is injected into the single-fractured granite until the fracture is activated based on the triaxial direct shear tests. The results show that injection process can significantly modify the shear stress distribution field, resulting in release of shear stress and relative slip between the opposite sides of the fractured surface. The injection-induced activation of fracture is strongly dependent on the stress states. When the normal stress increases, the injection-induced activation pressure increases, and the comparatively high normal stress can restrain the fracture activation. The fracture deformation mechanisms during injection are also discussed preliminarily with the experimental data. The sensitivity of shear stress to fluid injection increases with increase of shear stress level, while it decreases under high normal stress. The results can facilitate our understanding of the natural fracture activation behavior during fluid pressure stimulations.

Keywords: natural fracture; fluid injection; induced activation; triaxial direct shear test; hydraulic fracturing

1. Introduction

Hydraulic fracturing is critically important in improving productivity of deep oil/gas reservoirs, and has recently been widely used in geothermal reservoirs (Nemoto et al., 2008; Chuprakov et al., 2013; Kumari and Ranjith, 2019). Injection activities are frequently encountered in various industries, e.g. hydrocarbon exploitation, enhanced geothermal system developments, geological carbon storage, reservoir impoundment, and mining engineering (Deichmann and Giardini, 2009; McGarr et al., 2015; Cheng et al., 2019; Zhang et al., 2019b). Nevertheless, wastewater disposal associated with stimulation and production by injection into the subsurface could yield a higher risk of induced seismicity (Ellsworth, 2013), because this practice can activate pre-existing fractures and even large-scale faults. Rutqvist et al. (2015, 2016) conducted extensive researches on fault activation and induced seismicity in geological carbon storage. Doglioni (2018) classified the induced seismicity into four types, namely (I) graviquake, (II) reinjection quake, (III) hydrofracturing quake, and (IV) load quake; whilst fluid injection (type II) is possibly the most common mechanism of induced seismicity. Furthermore, some suggestions are proposed to reduce the probability of triggered seismicity (Zoback, 2012; Cornet, 2015; McGarr et al., 2015). In addition to large-scale faults, there are natural fractures in numerous formations that are the host medium for oil/gas accumulation (Montgomery et al., 2005), and complex hydraulic fracture networks may be created during treatment (Gale et al., 2007; Gu et al., 2012; Wang, 2019). Moreover, many studies (e.g. Huang et al., 2014; Selvadurai et al., 2018; Wang, 2019) have shown that the presence of natural fractures has significant impacts on the propagation of hydraulic fractures and associated flow characteristics.

Therefore, the interaction between hydraulic fracture and natural fracture has become a challenging issue over the recent years (Chuprakov et al., 2013; Wang et al., 2018; Cordero et al., 2019), which is basically characterized by arresting, crossing and slippage due to the influences of difference in horizontal principal stresses, approaching angle, and friction coefficient of fracture surface.

During hydraulic fracturing, the natural fractures are likely to be activated under shear stress, and more complex fracture networks will be created subsequently. This can maximize the stimulated reservoir volume and effectively improve the productivity of reservoirs (Warpinski and Teufel, 1987; Montgomery et al., 2005; Wang et al., 2018; Frash et al., 2019a). Guglielmi et al. (2015a, b) experimentally demonstrated that small-scale (micrometer-to-millimeter) fault activation may lead to a dramatic increase in permeability, and further revealed that fluid injection can generally trigger aseismic slip, followed by induced seismicity. Nemoto et al. (2008) conducted laboratory injection-induced slip experiments on pre-fractured granite, and the results show that stepwise slip and temporal increase in permeability occur in fractures during induced slip, and fracture roughness plays a significant role. Frash et al. (2016a, b; 2017; 2019b) performed a series of triaxial direct-shear tests with X-ray imaging on shale (or schist) and investigated the shear fracture propagation and flow behavior. Kohli and Zoback (2013) studied the effects of clay and organic contents on the frictional properties of shale reservoir rocks using laboratory friction experiments, indicating that the frictional strength can be reduced with increasing clay and organic contents. Creep experiments were also conducted on fault gouges in the double direct shear configuration to analyze fault slip evolution and hydrological properties under fluid injection (Scuderi et al., 2017; Scuderi and Collettini, 2018). Other observations have also been reported on evolution of fracture permeability during shearing and hydrostatic

compression (e.g. Carey et al., 2015; Fang et al., 2017; Selvadurai et al., 2018).

Nevertheless, the above-mentioned studies mainly focused on the fracture permeability evolution, frictional behavior, and fault activation-induced seismicity. Parts of the experimental achievements are completed under low stress conditions, which is only suitable for practical projects in shallow depth. In addition, studies on fracture or fault activation are mainly based on numerical methods (e.g. Shen et al., 2014; Rutqvist et al., 2016; Lisjak et al., 2017; Cordero et al., 2019; Zhang et al., 2019a, c) and in situ micro-seismic (MS) monitoring (e.g. Huang et al., 2014; Cheng et al., 2019), and few experimental observations has been reported. In this context, we proposed a new method to investigate the injection-induced activation characteristics of fracture, which can better facilitate our understanding of this issue. Taking the type II of induced seismicity (Doglioni, 2018) as an example, the stress conditions adopted in this method are almost consistent with the practical cases, as shown in Fig. 1.
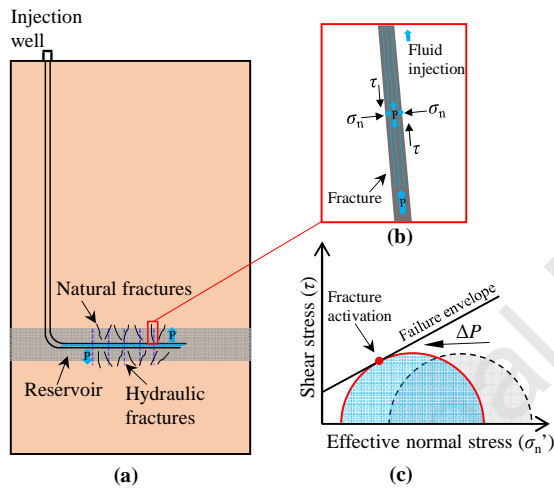

Fig. 1. (a) Schematic diagram of the injection well geometry used during hydraulic fracturing of fractured reservoir (modified after from Davies et al., 2013; Scuderi and Collettini, 2018). (b) Fluids infiltrating the natural fractures (blue arrows) due to hydraulic fracturing connection. The stress state around the fracture is presented. (c) Coulomb–Mohr diagram for the fracture before fluid infiltration (gray semicircle). As the fluid pressure increases (ΔP), the fracture may become instable, approaching the failure envelope (blue semicircle) and causing fracture activation.

2. Experimental set-up

2.1. Material

The studied granite was sampled from Suizhou, Hubei Province, China. The mineral composition of the sample was obtained using X-ray diffraction (XRD). The XRD results indicate that the granite is mainly composed of albite (55.31%), microcline (28.85%), quartz (14.35%), and biotite (1.49%). Fig. 2 shows an optical microscope image at 25 times magnification, with which the mineral texture can be clearly observed. According to the standard supported by the International Society of Rock Mechanics and Rock Engineering (Brown, 1981), cylindrical samples were prepared with a dimension of 100 mm × 50 mm (length × diameter), as shown in Fig. 3a. The intact rock sample has a uniaxial compressive strength (UCS) of 96.7 MPa and a Young's modulus (E) of 28.2 GPa. The indirect tensile strength is 3.5 MPa measured by Brazilian tests (ISRM, 1978). The gas permeability of the studied rock material was measured to be 2.35×10^{-17} m^2 under confining pressure of 2 MPa.

The Brazilian test was adopted to create a single fracture along the length of the granite sample (see Fig. 3b), in order to ensure the fracture with equal/similar roughness (Kunal et al., 2016; Tang et al., 2019).
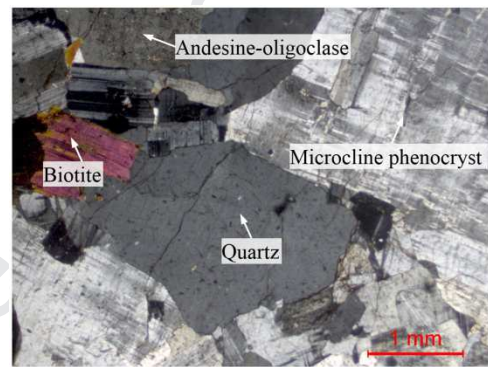

Fig. 2. Optical microscope image (×25).

2.2. Test procedures

The injection-induced fracture activation was investigated by triaxial direct shear test. The shear test device was placed in the hydro-mechanical coupling test system (Zhang et al., 2018), as illustrated in Fig. 4a. The shearing disc consists of two different materials (parts A and B) with different stiffnesses. Part A is rigid steel (i.e. forcing block) and part B is silicone with better elasticity and higher deformability. The two shearing discs are placed opposite on the upper and lower surfaces of the sample to convert the axial force into shear stress along the fracture surface, as shown in Fig. 3c. It is worth noting that the silicone filled between the forcing block and the end surfaces of sample provides negligible additional resistance to axial sample deformation (Samuelson and Spiers, 2012; Liu et al., 2020).
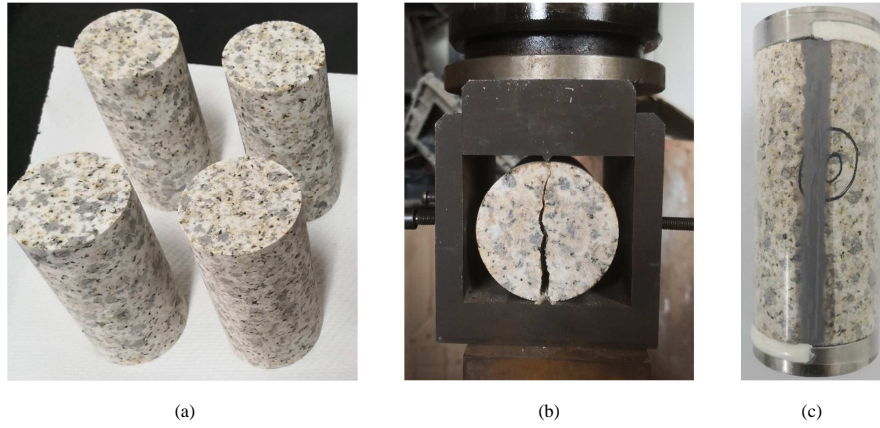
(a)   (b)   (c)

Fig. 3. (a) Granite samples, (b) the single fracture prefabricated using the Brazilian test, and (c) sample installation and sealing method.
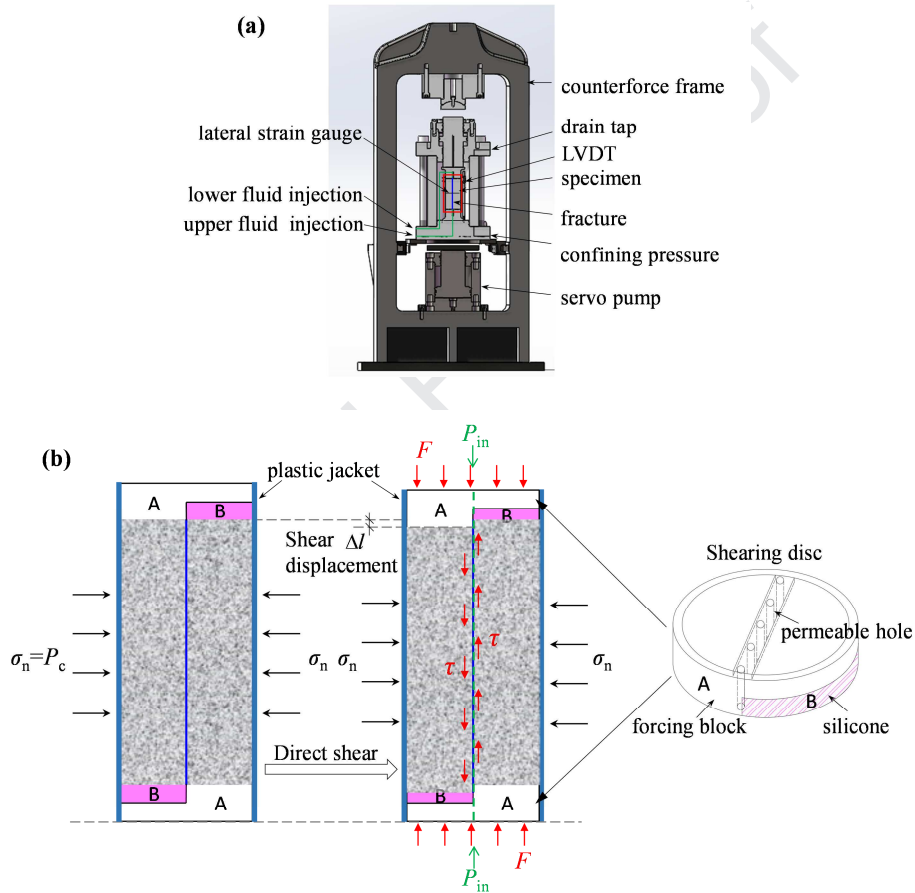

Fig. 4. Experimental set-up. (a) Hydro-mechanical coupling test system, and (b) details of conceptual view and principle of triaxial direct shear test. LVDT is Linear Variable Differential Transformers. P_c and σ_n respectively represent the confining pressure and the normal stress of fracture, which are equivalent. F is the axial force applied directly on the shearing discs. τ is the shear stress along the fracture converted from F. P_{in} is the fluid injection pressure.

This experiment was performed at room-temperature (25 °C) under different normal stresses (e.g. σ_n = 2, 5, 10, 20, 30, 40 MPa) in this work, using the following steps. Note that the proposed method is applicable to the most common mechanism of induced activation, i.e. fluid injection (Doglioni, 2018). The aim of this study is to verify the reliability of the proposed method and preliminarily discuss the characteristics of injection-induced fracture activation at laboratory scale. Taking σ_n = 20 MPa as an example, the loading stress path is shown in Fig. 5a.

(1) Step 1: Silicone is applied along the fracture on the sample outer surface for preliminary sealing in order to make the outer surface flat,

and then the sample and shearing discs are sealed with a plastic jacket (see Fig. 3c) to separate the sample from the hydraulic oil, and placed in the confining chamber (see Fig. 4a). The shear and normal displacements are measured via LVDTs and lateral strain gauge, respectively. The pressures are monitored by transducers with accuracy of ±0.1 MPa. The above experimental data can be recorded in a data acquisition center.

(2) Step 2: Apply confining stress (P_c) as isotropic stress by injecting silicon oil into the confining chamber at a rate of 0.5 MPa/min, which is equivalent to σ_n applied on the pre-existing fracture.

(3) Step 3: Apply axial force (F_i) to the desired level by running the

axial servo pump at a rate of 1 mL/min under constant normal stress, which results in a path that can be approximated as strain-controlling fashion (Carey et al., 2015; Frash et al., 2016a; Ding et al., 2020). The applied axial force can be converted into the shear stress (τ_i) on the fracture according to the following relation with reference to the method suggested by ISRM (Muralha et al., 2014):

$$\tau_i = \frac{F_i}{DL} \tag{1}$$

where D and L are the diameter and length of the sample, respectively.

Although Frash et al. (2019b, c) calibrated the shear stress obtained under the triaxial direct-shear condition using the direct shear tests of two Teflon semicylinder samples, the focus of this study is on the effects of fluid injection on fracture activation behavior. Hence, the additional resistance induced by the deformed silicone can be ignored, i.e. the applied axial force is considered to completely convert into shear stress in this context (Liu et al., 2020).

(4) Step 4: Water is injected at a rate of 0.5 mL/min into the fracture simultaneously through the permeable holes arranged along the diameter inside the shearing discs which are placed on the upper and lower ends of the sample (see Fig. 4b). As injection pressure increases, the pre-existing fracture will slip (i.e. activated) due to the continuous decrease of the effective normal stress. Low injection rate is employed in order to prevent a rapid increase of injection pressure (Nemoto et al., 2008).

(5) Step 5: The decrease in τ_i during injecting process can be regarded as an indicator that the fracture has been activated. Furthermore, the injection should be stopped and the fluid pressure must be unloaded to prevent excessive slip that will affect the subsequent tests.

(6) Step 6: Continue increasing τ_i and repeat steps 3–5, i.e. multi-stage shear procedure (Muralha et al., 2014). It is noteworthy that three or four shear stress levels (τ_i/τ_{max}) are selected under each normal stress to investigate the injection-induced activation of fracture under varied stress states, where τ_{max} refers to as the maximum shear strength.
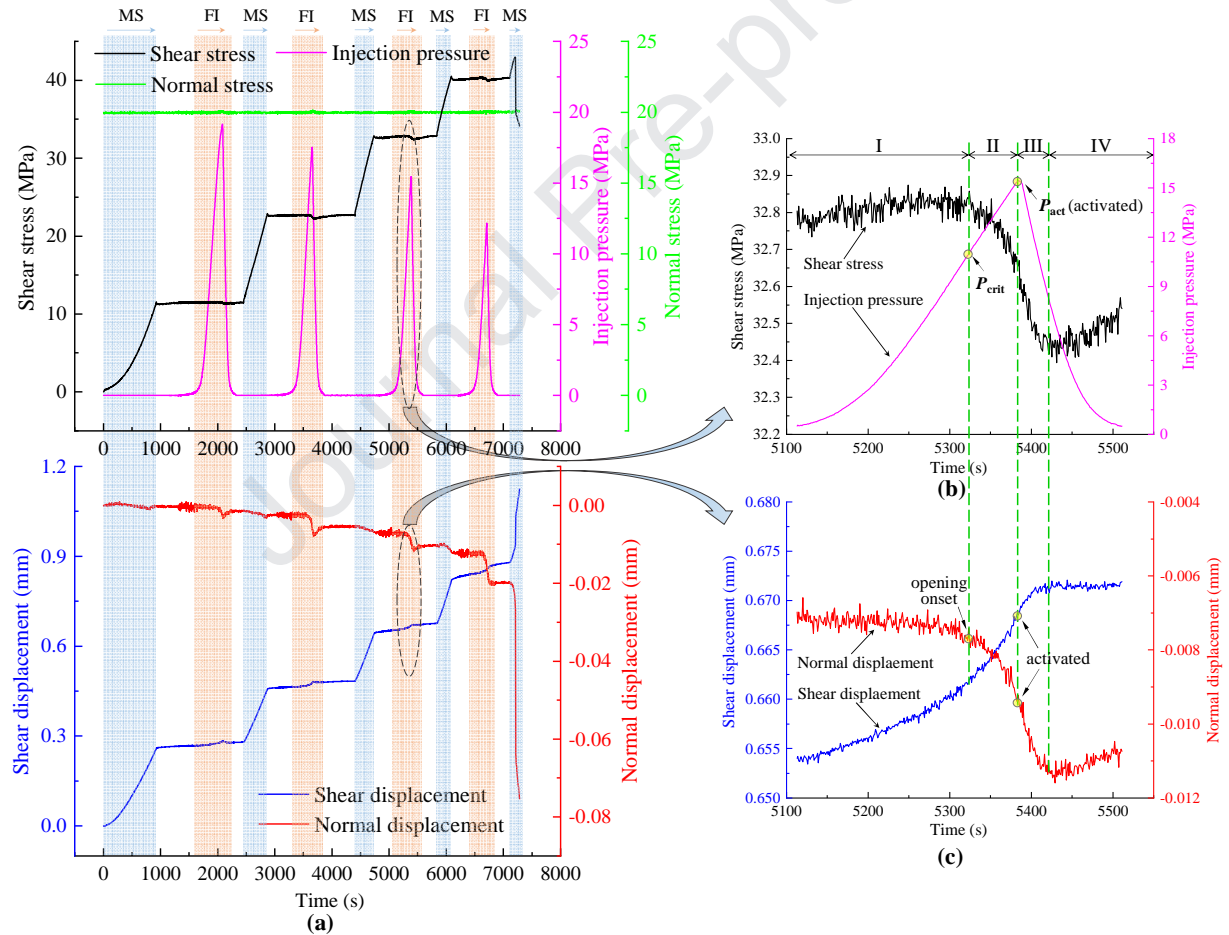

Fig. 5. (a) Diagram of the stress path at σ_n = 20 MPa (MS: mechanical shear, FI: fluid injection), (b) variation of shear stress during fluid injection, and (c) shear and normal displacements of fracture during fluid injection.

3. Results and discussion

3.1. Stress state and activation pressure of fracture

When the fracture is activated, the shear stress is noticeably reduced (see Fig. 5b), which is consistent with the observations of fractured hydro-shear test (Frash et al., 2019b). During injection, the shear stress mainly shows four phases: constant (phase I), gradually decreasing (phase II), sharply decreasing (phase III), and slowly increasing (phase IV). It shows that low initial injection pressure has a slight influence on the fracture stability, and the shear stress tends to be constant in phase I. As the injection pressure increases, the effective normal stress is continuously reduced and the fracture starts to slide, showing that the shear stress decreases gradually (phase II). Subsequently, the frictional instability on the fracture surface appears as a sharp decrease in shear stress. Although the injection pressure is gradually unloaded simultaneously, the fracture will further slide under the comparatively higher injection pressure, which presents continuous decrease in shear stress (phase III). In other words, there is hysteresis scenario in shear stress restitution. When the injection pressure is unloaded to a certain level, the shear stress starts to increase slowly (phase IV), due to the shear resistance recovering correlated to the increase of effective normal stress. This phenomenon is similar to the numerical results obtained by Kamali and Ghassemi (2018). Therefore, the injection process can significantly modify the shear stress distribution field of the fracture surface, causing release of shear stress and relative slip between the opposite sides of the fractured surface.

Fluid injection can result in reduction of effective normal stress, and Mohr's circle moves towards the sliding failure envelope until it triggers a slide (e.g. Ellsworth, 2013; Doglioni, 2018; Fan and Liu, 2019). Hence, injection-induced activation of fracture has a close relation with its stress states. When the normal stress is 2–20 MPa, the injection-induced activation pressure will decrease with increase of the shear stress. When the normal stress is comparatively high (e.g. $\sigma_n = 30$ and 40 MPa), the variations of injection-induced activation pressure are not evident upon increasing shear stress (see Fig. 6). The results suggest that the increase of σ_n can restrain the fracture activation to some extent. Obviously, as the normal stress increases, the injection-induced activation pressure increases, and approaches to the normal stress at $\sigma_n = 30$ and 40 MPa in this work. For practical reservoirs, the deeper the rocks, the higher the required injection pressure to activate the fractures, and the differential stresses also have a significant effect (Rutqvist et al., 2016).

3.2. Deformation characteristics of fracture during fluid injection

As shown in Fig. 5c, the shear displacement parallel to the direction of fracture increase gradually during injection process. On one hand, shear creep behavior occurs under constant shear stress (Scuderi et al., 2017), resulting in an increase in shear displacement. On the other hand, fluid injection decreases the effective normal stress and frictional resistance, thus the fracture is more prone to sliding with a gradual increase in shear displacement. It can also be seen that fluid injection can accelerate the slip rate of the fracture, showing a good agreement with the findings reported by Guglielmi et al. (2015a), Scuderi et al. (2017), and Frash et al. (2019b). Furthermore, the variation of fracture normal displacement is similar to that of shear stress, as shown in Fig. 5b and c. The fracture dilation is not obvious at the initial injection stage. As the injection pressure increases, the fracture dilation occurs and accelerates

gradually, indicating that the opening onset of the fracture occurs during sliding (Liu et al., 2020). This scenario possibly reflects the surface roughness and associated shear dilatation under the combined shear stress and continuous injection (Guglielmi et al., 2015a). After that, the dilation rate increases dramatically. When the fracture is activated, the shear displacement remains stable at the current position under the combined effects of reduced injection pressure and shear creep behavior. However, the fracture tends to close as the injection pressure is unloaded. There is also hysteresis scenario in recovery of normal displacement, similar to shear stress as mentioned previously. Therefore, injection-induced activation of fracture can be well characterized by the deformation mechanisms in this context.
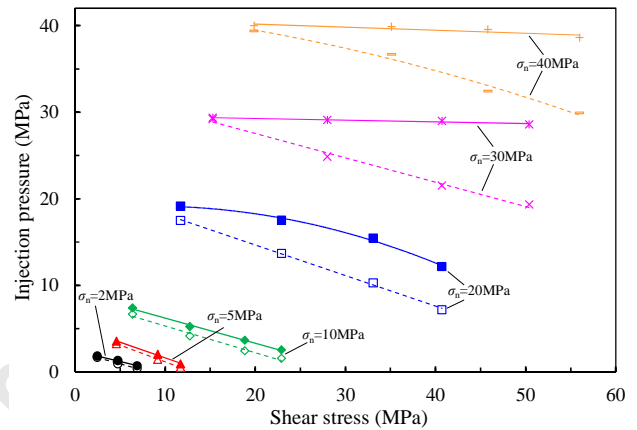

Fig. 6. Variations of the fracture activation pressure (solid line) and fracture critical-initiation pressure (dashed line) with shear stress under various normal stresses (σ_n).

3.3. Stress sensitivity of fracture activation

According to the above deformation analyses, the fracture slides continuously under constant shear stress in the multi-shearing stages, while the fracture opening onset occurs under a certain injection pressure. The inflection point of normal displacement is highly consistent with initial reduction of shear stress (i.e. the starting point of phase II), and the corresponding injection pressure can be considered as the fracture critical-initiation pressure (point P_{crit} in Fig. 5b). Prior to this, the fracture may be stabilized due to the cessation of injection, i.e. the stable sliding (phase I), and then the fracture can enter the unstable sliding (phases II, III) after the fracture opening onset with the significant variations in shear and normal displacements, as shown in Fig. 5b and c. Therefore, the fracture critical-initiation pressure of fluid injection results in a significant change in the stress state of the fracture surface. It is important in assessing the fracture activation behavior during injection.

In each experiment, the first injection-induced fracture activation can weaken the shear resistance of the fracture to some extent, including the damage of surface asperities, softening caused by fluid injection, and self-propped fracture formed after activation. As the shear stress increases gradually, subsequent repeated activation will significantly reduce the fracture critical-initiation pressure. This also well explains that the cyclic hydraulic fracturing can reduce the breakdown pressure and further enhance reservoir fracture connectivity (Zang et al., 2013; Patel et al., 2017). Therefore, the fracture critical-initiation pressure decreases with increasing shear stress (i.e. cumulative activation times), as shown in Fig. 6. This is distinguished from the variations of fracture activation pressure, especially under high normal stress (e.g. $\sigma_n = 30$ and 40 MPa), thus the

critical-initiation pressure can be utilized to predict the fracture activation behavior under injection-shearing coupled condition in this context. For comparison purpose, the fracture critical-activation coefficient (η) is proposed to evaluate the sensitivity of shear stress to injection process:

$$\eta = \frac{P_{\text{crit}}}{P_{\text{act}}} \tag{2}$$

where P_{act} is the injection pressure corresponding to fracture activation, P_{crit} represents the fracture critical-initiation pressure, which is the sign of shear stress decreasing and the transition from stable sliding to unstable sliding of fracture.

The larger η indicates that the higher injection pressure may be required for the initial release of shear stress, even close to the fracture activation pressure ($\eta = 1$), i.e. the shear stress is not very sensitive to fluid injection. The smaller η suggests that the response of shear stress is more sensitive during injection process. As shown in Fig. 7, the fracture critical-activation coefficient decreases monotonously under varied normal stresses, indicating that the sensitivity of shear stress to fluid injection increases with increase of shear stress level. Furthermore, the linear fitting slope decreases with increase of normal stress, suggesting that the shear stress is more sensitive when normal stress is lower; the fracture activation will be restrained when the normal stress is higher, and the sensitivity of shear stress is reduced subsequently.
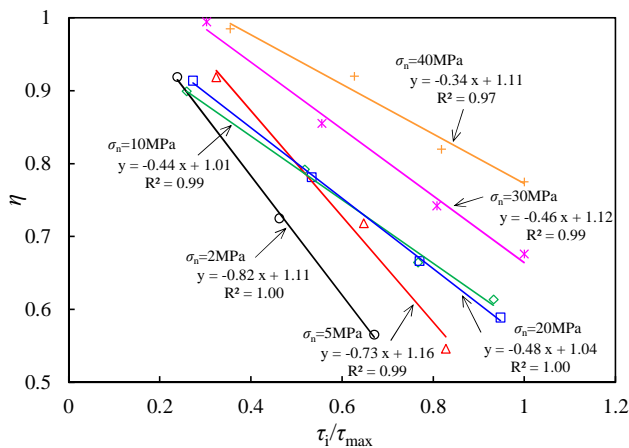

Fig. 7. Variations of the fracture critical-activation coefficient with shear stress level ($\tau_i/\tau_{\max}$) under various normal stresses (σ_n).

4. Conclusion

The main conclusions based on the experimental results can be drawn as follows:

(1) The new method proposed in this study is valid for investigation of injection-induced fracture activation at laboratory scale. The injection-induced activation of fracture is strongly dependent on the stress states. The fracture activation is mainly due to the fact that the fluid injection will decrease the effective normal stress, resulting in alteration of shear stress distribution field and releasing the shear stress accompanied by the relative slip between the opposite sides of the fractured surface.

(2) The injection-induced activation pressure increases with increase of the normal stress. It decreases with increase of the shear stress under the same normal stress. However, the activation of fractures can be restrained under high normal stress (e.g. σ_n = 30 and 40 MPa), and

the activation pressure approaches to the applied normal stress and remains almost constant with different shear stresses. The fracture critical-initiation pressure is defined based on the deformation characteristics and variation of shear stress, and it decreases with increasing shear stress under any normal stress. In addition, the sensitivity of shear stress to fluid injection increases with increase of shear stress level, but it can be reduced under comparatively higher normal stress, according to the proposed fracture critical-activation coefficient in this work.

(3) Higher injection pressure may be required for deeper fractured reservoirs to activate the pre-existing natural fracture system and to improve productivity during hydraulic stimulation. Furthermore, the injection activities should also be well controlled in combination with site-specific conditions to prevent large-scale fault activation-induced seismic hazards, especially in wastewater reinjection.

Nevertheless, in this method, the additional resistance resulting from the deformed silicone in the shearing discs is not considered. This may induce an overestimation of shear stress acting on the fracture, which should be addressed in future work. In addition, the settings of stress conditions in the following studies should focus on practical cases of reservoirs.

Declaration of Competing Interest

The authors declare that there is no conflict of interest in the present study.

References

Brown ET. Suggested methods for determining the uniaxial compressive strength and deformability of rock materials. In: Rock Characterization Testing and Monitoring—ISRM Suggested methods. Oxford: Pergamon Press; 1981.

Carey JW, Lei Z, Rougier E, Mori H, Viswanathan H. Fracture-permeability behavior of shale. Journal of Unconventional Oil and Gas Resources 2015;11:27–43.

Cheng GW, Li LC, Zhu WC, Yang TH, Tang CA, Zheng Y, Wang Y. Microseismic investigation of mining-induced brittle fault activation in a Chinese coal mine. International Journal of Rock Mechanics and Mining Sciences 2019;123. https://doi.org/10.1016/j.ijrmms.2019.104096.

Chuprakov D, Melchaeva O, Prioul R. Hydraulic fracture propagation across a weak discontinuity controlled by fluid injection. In: ISRM International Conference for Effective and Sustainable Hydraulic Fracturing. International Society for Rock Mechanics and Rock Engineering (ISRM); 2013.

Cordero JAR, Sanchez ECM, Roehl D, Pereira LC. Hydro-mechanical modeling of hydraulic fracture propagation and its interactions with frictional natural fractures. Computers and Geotechnics 2019;111:290–300.

Cornet FH. Earthquakes induced by fluid injections. Science 2015;348(6240):1204–5.

Davies R, Foulger G, Bindley A, Styles P. Induced seismicity and hydraulic fracturing for the recovery of hydrocarbons. Marine and Petroleum Geology 2013;45:171–85.

Deichmann N, Giardini D. Earthquakes induced by the stimulation of an enhanced geothermal system below Basel (Switzerland). Seismological Research Letters 2009;80(5):784–98.

Ding CD, Hu DW, Zhou H, Lu JJ, Lv T. Investigations of P-Wave Velocity, Mechanical Behavior and Thermal Properties of Anisotropic Slate. International Journal of Rock Mechanics and Mining Sciences 2020;127:104176. https://doi.org/10.1016/j.ijrmms.2019.104176.

Doglioni C. A classification of induced seismicity. Geoscience Frontiers 2018;9(6):1903–9.

Ellsworth WL. Injection-Induced Earthquakes. Science 2013;341(6142):1225942. https://doi.org/10.1126/science.1225942.

Fan L, Liu SM. Fluid-dependent shear slip behaviors of coal fractures and their implications on fracture frictional strength reduction and permeability evolutions. International Journal of Coal Geology 2019;212:103235. https://doi.org/10.1016/j.coal.2019.103235.

Fang Y, Elsworth D, Wang CY, Ishibashi T, Fitts JP. Frictional stability-permeability relationships for fractures in shales. Journal of Geophysical Research: Solid Earth 2017;122(3):1760–76. https://doi.org/10.1002/2016JB013435.

Frash LP, Carey JW, Lei Z, Rougier E, Ickes T, Viswanathan HS. High-stress triaxial direct-shear fracturing of Utica shale and in situ X-ray microtomography with permeability measurement. Journal of Geophysical Research: Solid Earth 2016a;121(7):5493–508.

Frash LP, Carey JW, Viswanathan HS, Gutierrez M, Hampton J, Hood J. Comparison of pressure, flow rate, stepped, and oscillatory control methods for fracture permeability measurements at triaxial stress conditions. In: 50th US Rock Mechanics/Geomechanics Symposium. American Rock Mechanics Association (ARMA); 2016b.

Frash LP, Carey JW, Ickes T, Viswanathan HS. Caprock integrity susceptibility to permeable fracture creation. International Journal of Greenhouse Gas Control 2017;64:60–72.

Frash LP, Welch NJ, Carey JW. Geomechanical evaluation of natural shear fractures in the EGS Collab Experiment 1 test bed. In: 53rd US Rock Mechanics/Geomechanics Symposium. American Rock Mechanics Association (ARMA); 2019a.

Frash LP, Carey JW, Welch NJ. EGS Collab Experiment 1 Geomechanical and Hydrological Properties by Triaxial Direct Shear. In: 44th Workshop on Geothermal Reservoir Engineering; 2019b.

Frash LP, Carey JW, Welch NJ. Scalable En Echelon Shear-Fracture Aperture-Roughness Mechanism: Theory, Validation, and Implications. Journal of Geophysical Research: Solid Earth 2019c;124(1):957–77.

Gale JFW, Reed RM, Holder J. Natural fractures in the Barnett Shale and their importance for hydraulic fracture treatments. American Association of Petroleum Geologists Bulletin 2007;91(4):603–22.

Gu H, Weng X, Lund J, Mack M, Ganguly U, Suarez-Rivera R. Hydraulic fracture crossing natural fracture at nonorthogonal angles: A criterion and its validation. SPE Production & Operations 2012;27(1):20–6. https://doi.org/10.2118/139984-PA.

Guglielmi Y, Cappa F, Avouac JP, Henry P, Elsworth D. Seismicity triggered by fluid injection-induced aseismic slip. Science 2015a;348(6240):1224–6.

Guglielmi YG, Henry P, Nussbaum C, Dick P, Gout C, Amann F. Underground Research Laboratories for conducting fault activation experiments in shales. In: 49th US Rock Mechanics/Geomechanics Symposium. American Rock Mechanics Association (ARMA); 2015b.

Huang J, Safari R, Mutlu U, Burns K, Geldmacher I, McClure M, Jackson S. Natural-Hydraulic fracture interaction: microseismic observations and geomechanical predictions. In: Unconventional Resources Technology Conference. Denver, CO, USA: Unconventional Resources Technology Conference; 2014.

ISRM. Suggested methods for determining tensile strength of rock materials. International Journal of Rock Mechanics and Mining Sciences & Geomechanics Abstracts 1978;15(3):99–103.

Kamali A, Ghassemi A. Analysis of injection-induced shear slip and fracture propagation in geothermal reservoir stimulation. Geothermics 2018;76:93–105.

Kohli AH, Zoback MD. Frictional properties of shale reservoir rocks. Journal of Geophysical Research: Solid Earth 2013;118(9):5109-25.

Kumari WGP, Ranjith PG. Sustainable development of enhanced geothermal systems based on geotechnical research—A review. Earth-Science Reviews 2019;199:102955. https://doi.org/10.1016/j.earscirev.2019.102955.

Kunal KS, Devendra NS, Ranjith PG. Effect of sample size on the fluid flow through a single fractured granitoid. Journal of Rock Mechanics and Geotechnical Engineering 2016;8(3):329–40.

Lisjak A, Kaifosh P, He L, Tatone BSA, Mahabadi OK, Grasselli G. A 2D, fully-coupled, hydro-mechanical, FDEM formulation for modelling fracturing processes in discontinuous, porous rock masses. Computers and Geotechnics 2017;81:1–18. https://doi.org/10.1016/j.compgeo.2016.07.009.

Liu ZB, Shao JF, Zha WH, Xie SY, Bourbon X, Camps G. Shear strength of interface between high performance concrete and claystone in the context of French radioactive waste repository project. Géotechnique, 2020. https://doi.org/10.1680/jgeot.19.P.098.

McGarr A, Bekins B, Burkardt N, Dewey J, Earle P, Ellsworth W, Ge S, Hickman S, Holland A, Majer E, Rubinstein J, Sheehan A. Coping with earthquakes induced by fluid injection. Science 2015;347(6224):830–1.

Montgomery SL, Jarvie DM, Bowker KA, Pollastro RM. Mississippian Barnett Shale, Fort Worth basin, north-central Texas: Gas-shale play with multi–trillion cubic foot potential. American Association of Petroleum Geologists Bulletin 2005;89:155–75. https://doi.org/10.1306/09170404042.

Muralha J, Grasselli G, Tatone B, Blümel M, Chryssanthakis P, Jiang YJ. ISRM Suggested Method for Laboratory Determination of the Shear Strength of Rock Joints: Revised Version. Rock Mechanics and Rock Engineering 2014;47:291–302.

Nemoto K, Moriya H, Mitsuma H, Tsuchiya N. Mechanical and hydraulic coupling of injection-induced slip along pre-existing fractures. Geothermics 2008;37(2):157–72.

Patel SM, Sondergeld CH, Rai CS. Laboratory studies of hydraulic fracturing by cyclic injection. International Journal of Rock Mechanics and Mining Sciences 2017;95:8–15. https://doi.org/10.1016/j.ijrmms.2017.03.008.

Rutqvist J, Rinaldi AP, Cappa F, Moridis GJ. Modeling of fault activation and seismicity by injection directly into a fault zone associated with hydraulic fracturing of shale-gas reservoirs. Journal of Petroleum Science and Engineering 2015;127:377–86. https://doi.org/10.1016/j.petrol.2015.01.019.

Rutqvist J, Rinaldi AP, Cappa F, Jeanne P, Mazzoldi A, Urpi L, Guglielmi Y, Vilarrasa V. Fault activation and induced seismicity in geological carbon storage—Lessons learned from recent modeling studies. Journal of Rock Mechanics and Geotechnical Engineering 2016;8(6):789–804.

Samuelson J, Spiers CJ. Fault friction and slip stability not affected by CO_2 storage: Evidence from short-term laboratory experiments on North Sea reservoir sandstones and caprocks. International Journal of Greenhouse Gas Control 2012;11:S78–S90.

Scuderi MM, Collettini C, Marone C. Frictional stability and earthquake triggering during fluid pressure stimulation of an experimental fault. Earth and Planetary Science Letters 2017;477:84–96.

Scuderi MM, Collettini C. Fluid injection and the mechanics of frictional stability of shale-bearing faults. Journal of Geophysical Research: Solid Earth 2018;123(10):8364–84.

Selvadurai APS, Zhang DJ, Kang YL. Permeability evolution in natural fractures and their potential influence on loss of productivity in ultra-deep gas reservoirs of the Tarim Basin, China. Journal of Natural Gas Science and Engineering 2018;58:162–77.

Shen WQ, He Z, Dormieux L, Kondo D. Effective strength of saturated double porous media with a Drucker–Prager solid phase. International Journal for Numerical and Analytical Methods in Geomechanics 2014;38(3):281–96.

Tang ZC, Zhang QZ, Peng J, Jiao YY. Experimental study on the water-weakening shear behaviors of sandstone joints collected from the middle region of Yunnan province, P.R. China. Engineering Geology 2019;258:105161. https://doi.org/10.1016/j.enggeo.2019.105161.

Wang WW, Olson JE, Prodanovic M, Schultz RA. Interaction between cemented natural fractures and hydraulic fractures assessed by experiments and numerical simulations. Journal of Petroleum Science and Engineering 2018;167:506–16.

Wang HY. Hydraulic fracture propagation in naturally fractured reservoirs: Complex fracture or fracture networks. Journal of Natural Gas Science and Engineering 2019;68:102911. https://doi.org/10.1016/j.jngse.2019.102911.

Warpinski NR, Teufel, LW. Influence of geologic discontinuities on hydraulic fracture propagation. Journal of Petroleum Technology 1987;39(2):209–20. https://doi.org/10.2118/13224-PA.

Zhang F, Zhao JJ, Hu DW, Skoczylas F, Shao JF. Laboratory Investigation on Physical and Mechanical Properties of Granite After Heating and Water-Cooling Treatment. Rock Mechanics and Rock Engineering 2018;51:677–94.

Zhang FS, Damjanac B, Maxwell S. Investigating Hydraulic Fracturing Complexity in Naturally Fractured Rock Masses Using Fully Coupled Multiscale Numerical Modeling. Rock Mechanics and Rock Engineering 2019a;52(12):5137–60.

Zhang LF, Lei XL, Liao, WL, Li JG, Yao YS. Statistical parameters of seismicity induced by the impoundment of the Three Gorges Reservoir, Central China. Tectonophysics 2019b;751:13–22.

Zhang X, Wu BS, Jeffrey RG, Yang DS, Chen WZ, Zhang FS. Changes of Slip Rate and Slip-Plane Orientation by Fault Geometrical Complexities During Fluid Injection. Journal of Geophysical Research: Solid Earth 2019c;124(8):9226–46.

Zang A, Yoon JS, Stephansson O, Heidbach O. Fatigue hydraulic fracturing by cyclic reservoir treatment enhances permeability and reduces induced seismicity. Geophysical Journal International 2013;195(2):1282–7.

Zoback MD. Managing the seismic risk posed by wastewater disposal. Earth 2012;57(4):38–43.

Changdong Ding obtained his BSc degree from Anhui University of Science and Technology, China (2017). He is a PhD student in Geotechnical Engineering from the Institute of Rock and Soil Mechanics, Chinese Academy of Sciences, since 2017. His research interests focus on rock mechanics and multi-field coupling mechanisms of deep fractured rocks. His research is under the joint supervision of Prof. Dawei Hu (IRSM, CAS) and Prof. Jianfu Shao (University of Lille, France).

Conflict of interest

The authors declare that there is no conflict of interest in the present study.